NANO LETTERS

Letter

pubs.acs.org/NanoLett

# Flexible Black Phosphorus Ambipolar Transistors, Circuits and AM Demodulator

Weinan Zhu,[†] Maruthi N. Yogeesh,[†] Shixuan Yang,[‡] Sandra H. Aldave,[†,§] Joon-Seok Kim,[†] Sushant Sonde,[†] Li Tao,[†] Nanshu Lu,[‡] and Deji Akinwande*,[†]

[†]Microelectronics Research Center, Department of Electrical and Computer Engineering, The University of Texas at Austin, Austin, Texas 78758, United States

[‡]Department of Aerospace Engineering and Engineering Mechanics and Texas Materials Institute, The University of Texas at Austin, Austin, Texas 78712, United States

[§]Polymer Science and Technology Department, University of the Basque Country, San Sebastian, Guipuzcoa 20018, Spain

Supporting Information

**ABSTRACT:** High-mobility two-dimensional (2D) semiconductors are desirable for high-performance mechanically flexible nanoelectronics. In this work, we report the first flexible black phosphorus (BP) field-effect transistors (FETs) with electron and hole mobilities superior to what has been previously achieved with other more studied flexible layered semiconducting transistors such as $MoS_2$ and $WSe_2$. Encapsulated bottom-gated BP ambipolar FETs on flexible polyimide afforded maximum carrier mobility of about 310 $cm^2/V{\cdot}s$ with field-effect current modulation exceeding 3 orders of magnitude. The device ambipolar functionality and high-mobility were employed to realize essential circuits of electronic systems for flexible technology including ambipolar digital inverter, frequency doubler, and analog amplifiers featuring voltage gain higher than other reported layered semiconductor flexible amplifiers. In addition, we demonstrate the first flexible BP amplitude-modulated (AM) demodulator, an active stage useful for radio receivers, based on a single ambipolar BP transistor, which results in audible signals when connected to a loudspeaker or earphone. Moreover, the BP transistors feature mechanical robustness up to 2% uniaxial tensile strain and up to 5000 bending cycles.

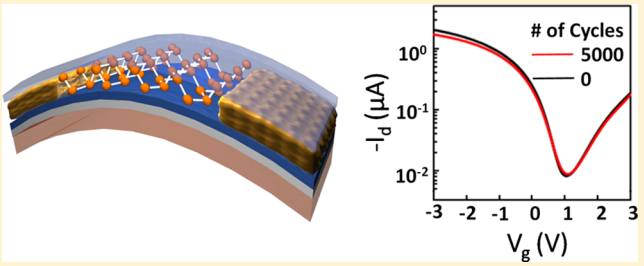


**KEYWORDS:** *phosphorene, flexible transistor, ambipolar conduction, frequency doubler, amplifiers, AM demodulator*

Two-dimensional (2D) crystalline nanomaterials have generated widely growing interest for diverse applications on mechanically soft flexible substrates owing to their generally inert surface, high elasticity, and thickness scalability down to a monolayer, which represents the ideal limit for electrostatic control, optical transparency, and bendability.[1−10] Over the past decade, graphene has been the foremost 2D atomic crystal investigated for flexible nanoelectronics with substantial advances in large-scale synthesis, device mobility, cutoff frequency, strain tolerance, and mechanical robustness.[3−6,11−13]

However, its lack of a bandgap results in a transistor that cannot be switched off by a gate voltage, an indispensable requirement for the vast majority of circuits in modern electronic systems.[3] Recently, transitional metal dichalcogenides (TMDs) such as $MoS_2$ and $WSe_2$ have emerged as suitable layered semiconductors that offer a sizable bandgap attractive for low-power electronics.[2,7,8,14,15] Nonetheless, despite promising theoretical prospects,[16,17] experimental TMD device mobilities have been relatively low, less than 50 $cm^2/V{\cdot}s$ on flexible substrates so far,[7,18−21] a value comparable to established amorphous materials such as metal oxide semiconductors that have transitioned into application products.[22−24]

To achieve higher carrier mobilities while retaining suitable field-effect current modulation, we have investigated black phosphorus (BP) devices on flexible substrates for the first time. Black phosphorus, otherwise known as phosphorene in the thin-film limit,[9,10] is a layered semiconducting 2D crystal similar to graphene but with a physically distinct puckered structure.[25,26] It is experiencing rapidly increasing research activity for a myriad of optoelectronic devices,[27−31] owing to its (i) high experimental mobility up to ∼1000 $cm^2/V{\cdot}s$[9] and (ii) thickness dependent direct bandgap spanning the infrared to visible regimes.[32]

In this work, flexible BP devices are realized on polyimide substrates affording maximum device mobility of ∼310 $cm^2/V{\cdot}s$, more than five times larger than the highest mobility achieved with flexible TMD transistors.[7,18−21] Ambipolar field-effect current modulation exceeds $10^3$ with sustained device perform-

**Received:** December 9, 2014
**Revised:** February 7, 2015
**Published:** February 25, 2015





DOI: 10.1021/nl5047329
*Nano Lett.* 2015, 15, 1883−1890

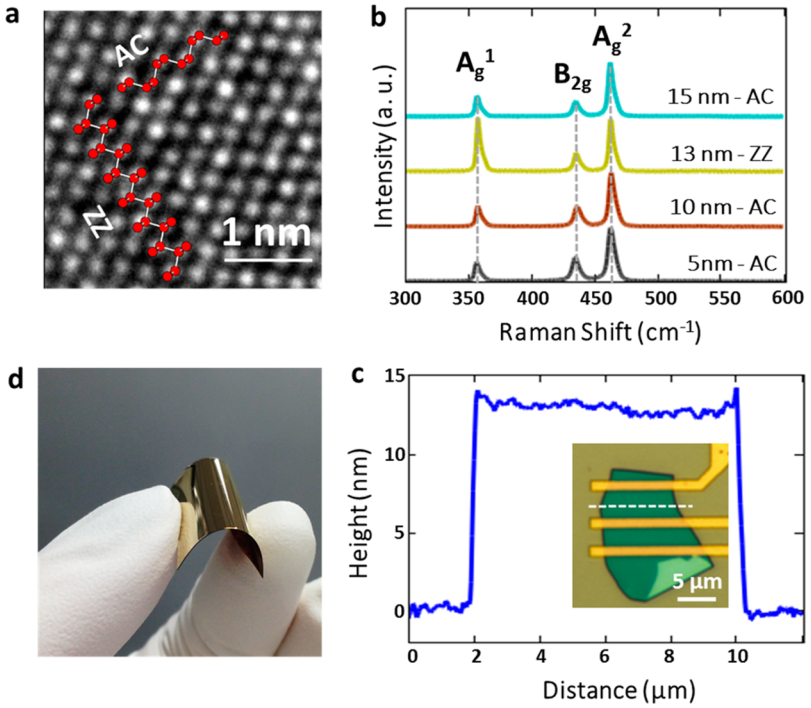


**Figure 1.** TEM, Raman, optical and AFM characterization. (a) HRTEM of few-layer black phosphorus. AC and ZZ edges are identified accordingly. (b) Raman spectroscopy of typical BP flakes explored in this work with thickness of 5, 10, 13, and 15 nm. A 532 nm linearly polarized laser was employed. The three black phosphorus characteristic peaks, $A_g^1$, $A_g^2$, and $B_{2g}$, are clearly resolved, and the intensity ratio among the three peaks indicate that the in-plane laser polarization is along either the armchair (AC) or zigzag (ZZ) directions. (c) AFM height profile of a BP flake with measured AFM thickness of 13 nm corresponding to the dashed line in the inset, which is the optical image of the bottom-gate transistors based on this flake. (d) Optical image of few-layer BP devices on a flexible substrate.

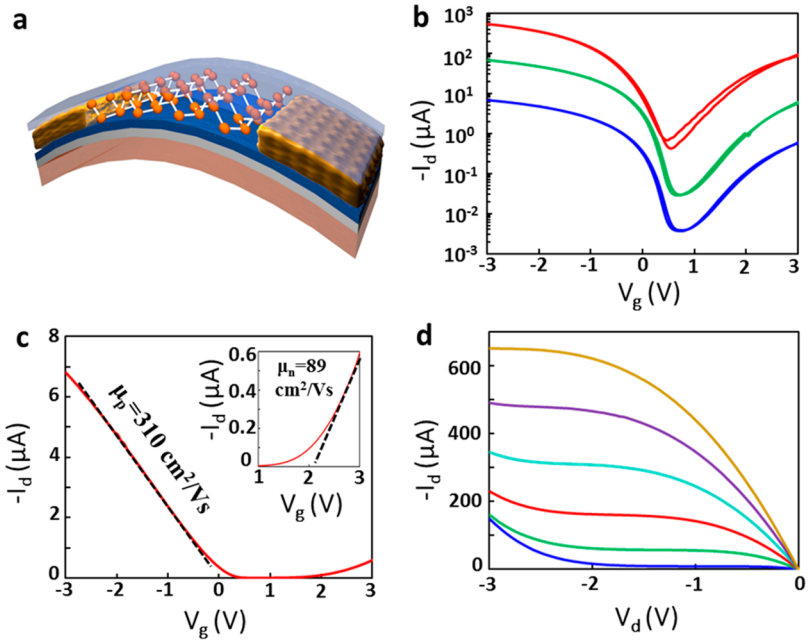


**Figure 2.** Schematic and current−voltage characteristics of bottom-gate (BG) BP FETs on flexible substrate. (a) Simplified illustration of the device structure of flexible BG BP FET on PI substrate (not to scale). Ti/Pd/$Al_2O_3$ with 3 nm/50 nm/25 nm thickness was deposited as global bottom gate and gate dielectric stack. Ti/Au with 1.5 nm/70 nm thickness is lithographically formed as the metal contacts to the semiconducting BP channel. A top-side layer of 25 nm $Al_2O_3$ was deposited for device encapsulation. (b) Log plot of the transfer characteristics of encapsulated BG BP FET on PI, showing >$10^3$ on/off ratio, negligible hysteresis, and clear ambipolar character. Drain bias is $V_d$ = −10 mV, −100 mV and −1 V from bottom to top. Flake thickness is 15 nm, and $W/L$ = 10.6 $\mu$m/2.7 $\mu$m. (c) Linear plot of transfer characteristics at $V_d$ = −10 mV, showing low-field hole $\mu_h$ of 310 cm$^2$/(V s). Electron mobility ($\mu_e$) was extracted to be 89 cm$^2$/(V s) for this device, as is shown in the inset. (d) Output curves of the same device displaying current saturation. Gate bias, $V_g$ = 0 to −2.5 V from bottom to top, with a step size of −0.5 V.



DOI: 10.1021/nl5047329
*Nano Lett.* 2015, 15, 1883−1890

ance at 2% uniaxial strain and, after 5000 bending cycles, that is ultimately limited by the mechanical robustness of the gate dielectric.[7] Based on the ambipolar functionality and high mobility, we demonstrate several circuit blocks essential for future flexible nanoelectronic systems, including ambipolar inverter, frequency doubler, and inverting and noninverting analog amplifiers with voltage gains of ~8.7, more than two times higher than previous flexible thin-film amplifiers.[15,33,34] Lastly, a flexible amplitude-modulated (AM) demodulator was developed based on a single BP ambipolar transistor that yielded audible signals when connected to a loudspeaker or earphone. Our results indicate that black phosphorus is the most promising layered semiconductor for flexible nanoelectronics.

**Results and Discussion.** The crystalline nature of multilayer black phosphorus investigated in this work was verified with both high-resolution transmission electron microscopy (HRTEM) and Raman spectroscopy. Figure 1a displays the HRTEM top-view image of a typical multilayer BP flake highlighting both the arm-chair (AC) and zigzag (ZZ) edges. Raman spectroscopy of several mechanically exfoliated samples (Figure 1b) with thickness between 5 and 15 nm revealed the three characteristic vibrational modes ($A_g^1$, $B_{2g}$, and $A_g^2$) of black phosphorus further confirming the chemical identity of the thin films. Owing to the puckered anisotropic crystal structure of black phosphorus (Supporting Information Figure S1a), Raman intensity ratios among the three peaks are highly sensitive to its in-plane crystal orientation.[35,36] This light−matter orientation dependence can be routinely used to determine the orientation of BP flakes with respect to the charge transport direction in fabricated transistor devices. The Raman spectra featured in Figure 1b represents the AC direction for flakes with thickness of 5, 10, and 15 nm, and the ZZ direction for the 13 nm flake profiled in the inset of Figure 1c. Detailed Raman spectra with one BP crystal flake oriented along both the AC and the ZZ directions can be found in the Supporting Information, Figure S1b. To achieve high-speed charge transport in BP transistors, it is known that the AC direction affords lower effective mass and correspondingly higher mobilities compared to other crystal orientations.[25,37] In this work, all Raman spectra were measured after device fabrication and electrical measurements were completed in order to avoid potential damage to the BP flakes from the Raman laser.

To fabricate the transistor devices, few-layer semiconducting black phosphorus was first mechanically exfoliated from commercial supplies (from Smart-elements) onto polyimide (PI) substrate as channel material for bottom gate field-effect transistors (FETs). Due to the lack of established synthesis method for either monolayer or multilayer black phosphorus, exfoliation was employed as an effective route for obtaining BP flakes (thickness ≤15 nm) with micrometer lateral dimensions. Figure 1c displays the optical image and atomic force microscopy (AFM) thickness measurement of a typical exfoliated BP flake with a smooth and uniform surface, necessary features for nanoelectronic devices. An optical image of a flexible PI substrate with encapsulated BP electronic devices is shown in Figure 1d with inherent flexibility and stability for ambient operation.

The transistor device structure on flexible polyimide developed in this work is illustrated in Figure 2a, featuring an embedded bottom-gate for field effect,[4,7] and $Al_2O_3$ encapsulation for air stability.[38,39] Commercial PI (Kapton) was utilized as the flexible substrate followed by double-sided spin-coated cured PI to achieve nanoscale smooth surfaces with roughness of ~1−3 nm.[40] The global bottom-gate was realized by electron beam evaporation of Ti/Pd metal stack with 3 nm/50 nm thickness. Then, 25 nm $Al_2O_3$ deposited by atomic layer deposition (ALD) was used as bottom gate dielectric, which yields a measured gate oxide capacitance of 0.21 $\mu F/cm^2$ and affords routine visual identification of suitable BP flakes by optical microscopy. BP flakes were exfoliated onto the substrate and immediately covered with poly(methyl methacrylate) (PMMA), an electron beam resist to prevent air degradation of black phosphorus during device fabrication. Accurate flake thickness was determined by AFM after completion of electrical measurement experiments. Source and drain contacts were formed by electron beam lithography and deposition of 1.5 nm/70 nm Ti/Au metal stack, which was selected due to its high work function and reduced injection barrier to the valence band.[41−43] Afterward, another layer of 25 nm $Al_2O_3$ was deposited by ALD to encapsulate the BP devices, which proved effective in maintaining stable electrical properties over the weeks-long duration of experiments under ambient conditions (Supporting Information, Figure S2).

Outstanding device performance including high mobility, strong current saturation, and ambipolar transport were observed at room temperature in ambient environment for the encapsulated flexible BP transistors. The transport direction aligned well with the AC crystal orientation based on the Raman spectrum (Figure 1c) taken after the device fabrication. Transfer characteristics with negligible hysteresis were achieved (Figure 2b) owing to the effective ALD encapsulation and protection against moisture adsorption.[38,39] Drain current modulation approaching 4 orders of magnitude was obtained on BP device with film thickness of 15 nm, which is much higher than recently reported values of about ten.[10,35] We attribute this improvement to the $Al_2O_3$ encapsulation layer that effectively reduces the residual charge adsorbed from the ambient environment at the black phosphorus surface, thereby affording greater gate control in switching the device. With negligible electrical hysteresis, charge transport can be accurately analyzed. The extracted low-field hole mobility ($\mu_h$) using the Y-function linear slope method[44] was 310 $cm^2/(V{\cdot}s)$, which is much higher than state-of-the-art semiconducting TMD, organic and metal oxide flexible transistors.[7,18−21] A comparison of our flexible BP and the highest reported flexible thin-film semiconductor transistors with respect to carrier mobility and current modulation are listed in Table 1. (Electrical performance statistics of 19 flexible BP transistors are shown in Supporting Information Figure S3.) In addition to the high hole mobility that is superior to that of semiconducting p-type TMDs, ambipolar black phosphorus can afford field-effect electron mobility ($\mu_e$) exceeding that of n-type TMDs as shown in Table 1, where the electron mobility of BP FET (~89 $cm^2/(V{\cdot}s)$) is ~3 times higher than the highest reported value for contemporary $MoS_2$ flexible transistors.[7] This $\mu_e$ is also the highest number reported for BP transistors so far, despite the fact that the present BP devices are not optimized for electron transport, indicating overall n-type device improvement can be expected with contacts that preferentially favor electron transport.[42,43,45]

In addition, strong saturation was achieved in the output characteristics (Figure 2d), a necessary feature for realizing high cutoff frequencies for power gain and high-performance analog amplifiers and circuits.[3,4] The attractive device metrics of high


DOI: 10.1021/nl5047329
Nano Lett. 2015, 15, 1883−1890

**Table 1. Basic Comparison of Flexible Thin-Film Semiconducting Transistors Including Black Phosphorus, Layered Metal Dichalcogenides, Organic Semiconductors, and Metal Oxide Semiconductors[a]**

| material | FET mobility ($cm^2/V·s$) $\mu_e$ | $\mu_h$ | ON/OFF ratio | film thickness (nm) | transport type |
|---|---|---|---|---|---|
| black phosphorus (this work) | 89 | 310 | $10^3$–$10^4$ | 15 | ambipolar |
| | 3 | 180 | $10^4$–$10^5$ | 5 | ambipolar |
| $MoS_2$ ref 7 | 30 | | $10^7$–$10^8$ | 10 | n-type |
| $WSe_2$ ref 18 | 24 | 45 | $10^7$ | 1.5 | ambipolar |
| $SnS_xSe_{2-x}$ ref 19 | 12 | | $10^6$ | 5 | n-type |
| pentacene ref 20 | | 8.85 | $10^3$–$10^4$ | 65 | p-type |
| InGaZnO ref 21 | 76 | | $10^5$ | 23 | n-type |

[a]The table features the state-of-the-art device metrics for each thin-film material. Data is for micrometer-sized devices at room temperature.

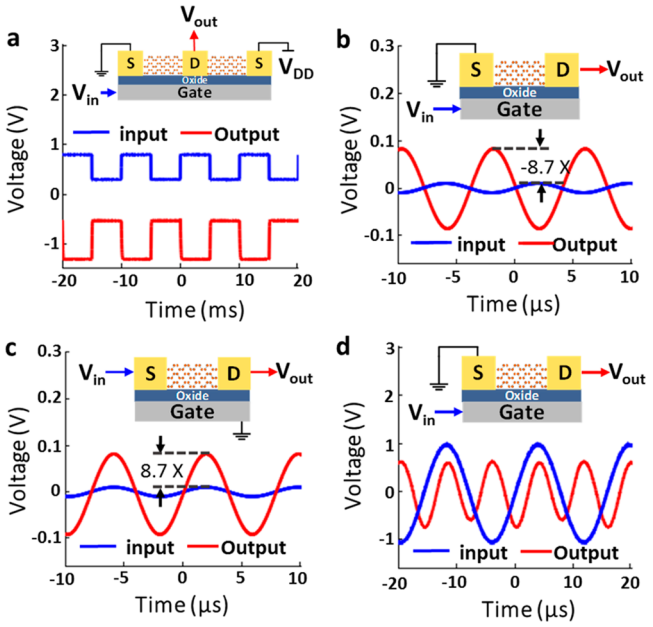


**Figure 3.** Basic digital and analog circuits based on flexible BP transistors. (a) Ambipolar digital inverter. DC bias $V_g$ = −0.46 V and $V_{dd}$ = −2 V. Input pulse oscillates at 100 Hz with peak-to-peak amplitude ($V_{pp}$) of 0.5 V. Inverter output pulse showing a gain of ∼1.6. (b) Inverting voltage amplifier (i.e., common-source amplifier), and (c) noninverting voltage amplifier (i.e., common-gate amplifier). At a symmetric DC bias of $V_{gs}$ = −1.6 V and $V_{ds}$ = −2.1 V for both circuits, the small-signal voltage gain for both amplifiers is ∼|8.7|. Simplified AC signal schematics of the device circuit and electrical connections are shown in the insets. (d) Ambipolar single FET frequency doubler. Input signal is 64 kHz sinusoid with $V_{pp}$ = 2 V. Output signal oscillates at the double frequency (128 kHz) with a voltage gain of ∼0.7. $V_g$ = 0 V and $V_d$ = −1 V.

mobilities, strong current saturation, direct bandgap and sizable on/off ratio motivates the interest in black phosphorus for both high-speed digital and analog thin-film transistors and circuits on flexible substrates. With this in mind, electronic circuits that can provide essential functions including ambipolar inverter, frequency doubler and demodulator, and inverting and noninverting voltage amplifiers were successfully realized based on single/double BP transistors. The capability to realize functional circuits based on a small count of BP transistors is particularly attractive for the nascent flexible nanoelectronics applications where large-scale integration has not yet been developed unlike modern semiconductor technology. Simplified schematics illustrating the signal flow for the four types of circuits demonstrated in this work are shown as inserts in Figure 3.

The inverter device structure enabled by the ambipolar transport characteristics in fabricated BP FETs as well as the high drain current modulation, was successfully achieved by splitting the minimum conduction points of two series transistors, similar in concept to graphene ambipolar inverters.[46] For ambipolar inverters, a relatively thicker BP flake ($t$ = 15 nm) was chosen for its favorable lower bandgap of ∼0.3 eV,[10,32] a small value that typically leads to ambipolar transport characteristic due to the relatively lower Schottky barrier height for the minority carrier (electron) injection compared to thinner films that will present a larger Schottky barrier and reduced ambipolarity.[42,43] Two identical bottom gate transistors fabricated from the 15 nm thin flake were combined into a complementary inverter circuit, with the global bottom gate as the input, and the center terminal as the output (Figure 3a insert). Clear inverting functionality can be seen in Supporting Information Figure S4a with peak inverter gain of ∼|4.6| for $V_g$ = −0.46 V and $V_{dd}$ = −2 V (Supporting Information Figure S4b). Based on the ambipolar inverter, a push−pull amplifier, which is a fundamental circuit for output voltage stages,[47] was realized as shown in Figure 3a. An input pulse signal with peak-to-peak amplitude ($V_{pp}$) of 0.5 V was connected to the gate input, and the amplified inverted signal was observed at the center output terminal with an output/input voltage gain of ∼1.68 (Figure 3a). The push−pull amplifier operates at a maximum frequency of 100 Hz, which is limited by the very large parasitic capacitance from the bottom gate structure. By optimizing the device structure, for example, utilizing isolated top gate or patterned bottom gate electrodes,[4,48] higher frequency operation will be accessible.[15,49] Previously, we showed in ref 4 that patterned embedded-gate graphene flexible transistor with 0.5 $\mu$m channel length afforded intrinsic cutoff frequency of 25 GHz. By replacing the graphene channel material with black phosphorus, we estimate that similar optimized 0.5 $\mu$m BP flexible transistor could yield cutoff frequency exceeding 1 GHz based on the experimental mobility of 310 $cm^2/V·s$ achieved in this work. Moreover, Wang et al. has recently reported 20 GHz cutoff frequency for 0.3 $\mu$m BP FET on hard substrate,[48] further highlighting the high frequency prospects of this nanomaterial.

Inverting and noninverting single-transistor amplifiers (Figure 3b and c) are among the most important circuit units for analog signal processing and require both current saturation in the device output characteristics and high transconductance ($g_m$) in order to achieve high voltage gain.[3,7] In this work, both inverting (i.e., common-source) and noninverting (i.e., common-gate) configurations were realized from the same BP transistor. The voltage bias was at a symmetric value of $V_{gs}$ = −1.6 V and $V_{ds}$ = −2 V, where the intrinsic gain ($g_m/g_{ds}$) for the device was around its peak value (Supporting Information Figure S5b). For the inverting amplifier, the source was grounded (Figure 3b) and the output collected at the drain terminal, which resulted in a voltage gain ($A_v = V_{out}/V_{in}$) of −8.7 with a small-signal input of $V_{pp}$ = 20 mV applied at the gate terminal. The amplifier load consisted of a 1 MΩ resistor


DOI: 10.1021/nl5047329
Nano Lett. 2015, 15, 1883−1890

from the oscilloscope, and a shunt inductor-series capacitor bias-tee network for separating DC and AC signals.[50] For the noninverting amplifier (Figure 3c), the bottom gate was grounded and the source and drain served as the input and output terminals respectively, resulting in positive voltage gain of 8.7 for the same small-signal input and load as described for the inverting amplifier. The identical amplifier gains with opposite polarity reflects the symmetry of the gate-source terminal afforded in a 2D semiconductor, in contrast to a bulk semiconductor where the bulk terminal can introduce significant asymmetry between the common-gate and common-source configurations due to the body effect.[51] Previous flexible thin-film transistor based amplifiers achieved voltage gains <4;[15,33,34] hence, the present BP FETs have the highest circuit amplification factor reported so far, which signifies the promising potential of black phosphorus for flexible analog electronics.

A single-transistor frequency doubler is highly desirable for analog circuits owing to the benefits of low transistor count, reduced power consumption, and the absence of device matching, a stringent requirement for frequency multipliers based on transistor pairs.[52] Previously, graphene frequency doublers based on the square-law ambipolar property of Dirac Fermions have been shown to be suitable for single-transistor frequency doubling with a substantially cleaner output spectrum compared to conventional diode or transistor multipliers that are based on current−voltage nonlinearities.[5,53,54] Here, we demonstrate for the first time that flexible BP transistors can suitably function as a single-transistor frequency doubler based on the ambipolar charge transport of elementary Fermions (see Supporting Information for the analysis of ambipolar BP frequency doubler). The main distinction between ambipolar black phosphorus and ambipolar graphene (under ideal electron−hole symmetry) arises at the ambipolar symmetry point that reflects a diffusive (exponential) transport for black phosphorus, and a drift (linear) transport for graphene. Although graphene can afford a higher conversion gain due its more optimum square-law properties,[53] black phosphorus can offer lower power and higher power efficiency owing to its lower off current and DC power dissipation, respectively. Our primary purpose here is to investigate frequency doublers based on black phosphorus and subsequently exploit the ambipolar property for realizing an AM demodulator on a flexible substrate, of great importance for communication and connectivity in future flexible smart systems.[1]

For frequency doubler operation, the BP transistor device shown in Figure 3d was biased at $V_d = -1$ V to realize a more symmetric transfer characteristic near the minimum conduction point, $V_{min} = 0.54$ V, which was slightly adjusted to $V_g = 0$ V to account for the asymmetry between electron and hole transport, similar to previous report on asymmetric graphene frequency doubler.[55,56] Sinusoidal frequency doubling was achieved with a conversion gain of 0.72 between output and input voltages with the input frequency at 64 kHz and an input $V_{pp}$ of 2 V as shown in Figure 3d.

On the basis of the ambipolar property of our BP transistors and the above-mentioned realization of frequency doubler, we developed a flexible BP AM demodulator. The BP AM demodulator is a single-transistor circuit that demodulates AM signals, which can be monitored electrically via an oscilloscope or acoustically via a loudspeaker. Future flexible BP AM radio receiver[57] can be realized based on our successful demonstration of an AM demodulator, the schematic of which is shown in Figure 4a. BP transistor was biased at $V_g = 0$ V and

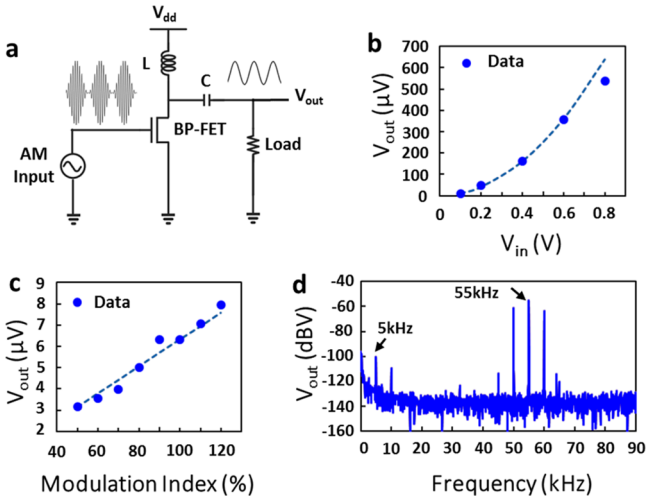


**Figure 4.** Demonstration of an AM demodulator based on flexible BP FET. (a) Schematic representation of an ideal AM demodulator system based on BP FET operating at the ambipolar point. An AM modulated low-frequency signal constituted the input drive to the gate of the ambipolar FET. BP FET at the ambipolar point can be approximated to second-order as a square law device resulting in self-mixing that produces a demodulated output that can be observed in an oscilloscope or heard via a loudspeaker. (b) Dependence of demodulated baseband output (5 kHz sinusoid) on $V_{pp}$ of the input carrier signal (55 kHz sinusoid). The symbols are the measured demodulated output signal dependence, which is in agreement with the expected square-law quadratic relation indicated by the dashed line. (c) Dependence of the demodulated output baseband signal on the modulation index displays a linear trend (dash line) as expected from square law demodulator theory. (d) Output spectrum of the ambipolar transistor demodulator showing the demodulated baseband signal (5 kHz) and the modulated carrier feed-through (55 kHz). Input carrier $V_{pp} = 100$ mV.

$V_d = -1$ V, the same conditions as the frequency doubler. The second-order square law demodulator analysis of ambipolar black phosphorus is detailed in the Supporting Information. Baseband audio signal was AM modulated onto a carrier frequency (55 kHz) as input to the gate terminal, while the output demodulated signal at the drain terminal was sent either to a loudspeaker or an oscilloscope. To elucidate the square law demodulator performance of the flexible BP AM demodulator, a 5 kHz sinusoidal baseband signal was applied and its corresponding output spectrum was evaluated using an oscilloscope with high resolution fast Fourier transform (FFT). With the same DC bias as mentioned earlier and with varying carrier signal amplitude from 100 mV to 800 mV, the output amplitude of the demodulated 5 kHz signal increased quadratically in agreement with the expected square law behavior as is shown in Figure 4b. In addition, the linear dependence of the baseband output amplitude on the modulation index was observed as expected for a square law device (Figure 4c). The FFT output signal spectrum for a 100 mV input peak-to-peak carrier amplitude at 100% modulation index is shown in Figure 4d. The carrier feed-through present in the spectrum is due to the asymmetry of the BP ambipolar transistor, consequently resulting in odd harmonics.[53] A media file (Supporting Information Video 1) demonstrates the working BP AM demodulator. Further information about the


DOI: 10.1021/nl5047329
Nano Lett. 2015, 15, 1883−1890

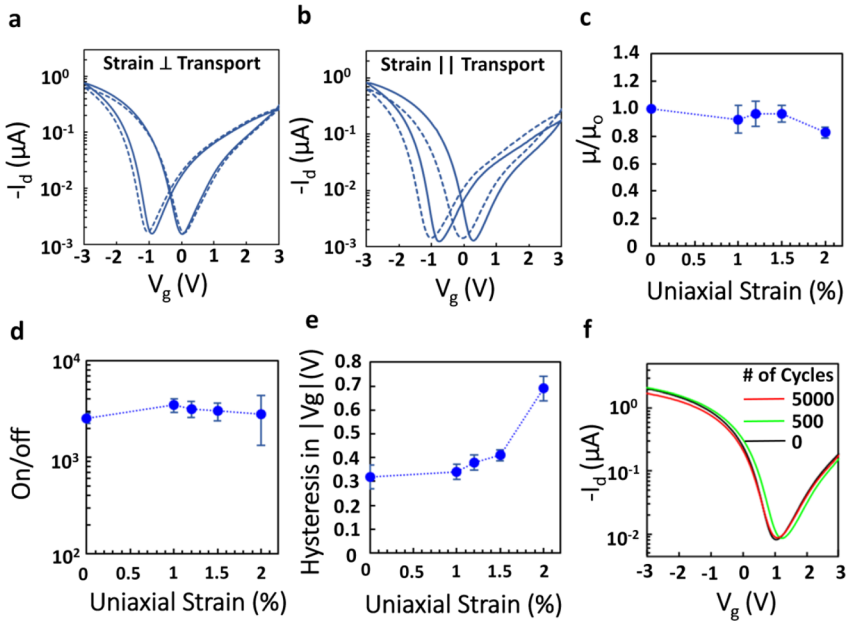


**Figure 5.** Uniaxial tensile evaluation of BP flexible transistors under mechanical bending. (a) and (b) are comparison between transfer curves before (solid line) and after (dash line) applied perpendicular ($\varepsilon_\perp$) and parallel ($\varepsilon_\parallel$) uniaxial tensile strain of ~1.5%, respectively. Larger hysteresis was observed when the applied strain is parallel to the direction of charge transport. Device statistics including (c) normalized low-field hole mobility $\mu_h$, (d) on/off ratio, and (e) voltage hysteresis under increasing tensile strain in the parallel direction ($\varepsilon_\parallel$). Device performance degradation begins at ~2% strain, which is attributed to residual strain in the substrate and the $Al_2O_3$ gate dielectric and passivation layers. (f) Multicycle three-point bending results, showing the robustness of BP device transfer characteristics before and after 500 and 5000 bending cycles. The BP devices were at the center of curvature of the substrate for the bending experiments.

measurement system setup is provided in the Supporting Information Figure S6.

In addition to device and circuit performance, transistor robustness under applied strain is another criteria of central importance for flexible electronics. In this work, the robustness of flexible BP transistors and demodulator with respect to both uniaxial tensile strain loading and multicycle bending were evaluated for the first time. All the electrical characteristics were measured ex situ (after the applied strain was released), a straightforward and conventional method for evaluating the mechanical robustness of flexible devices.[4,7,58] In this work, crystal orientation dependent transport anisotropy was not considered due to the range of tensile strain applied (≤2%), which is not expected to result in significant crystal orientation dependent device performance.[59−61]

With uniaxial tensile strain applied, it is necessary to compare the effect of parallel ($\varepsilon_\parallel$) and perpendicular ($\varepsilon_\perp$) strains on flexible BP transistors. $\varepsilon_\parallel$ ($\varepsilon_\perp$) is defined as the case when the uniaxial tensile strain is aligned parallel (perpendicular) to the direction of electrical transport in the transistor. The transfer characteristics measured after 1.5% tensile strain for both $\varepsilon_\perp$ (Figure 5a) and $\varepsilon_\parallel$ (Figure 5b), reveal stable device properties with $\varepsilon_\parallel$ showing a slightly higher effect on device characteristics resulting in a relatively larger shift in both the threshold voltage ($V_t$) and $V_{min}$. One plausible reason for this effect is the significant reduction of local longitudinal strain in BP channel induced by $\varepsilon_\perp$ compared to $\varepsilon_\parallel$ due to the Poisson effect.[62,63] The Poisson ratio of the polyimide substrate is ~0.34. Moreover, in the transfer characteristics measured after 1.5% parallel tensile strain, no significant change in the basic device parameters such as $I_{on}$, current on/off ratio and carrier mobility was observed. The extracted mobility variation from Figure 5b is within 3.7% of its initial value.

To further investigate the performance robustness of flexible BP transistors, transfer and output characteristics were evaluated under increasing tensile strain $\varepsilon_\parallel$, which will result in higher effect on device performance as above-mentioned, up to 2% corresponding to 3 mm bending radius. Statistics for electrical parameters of interest, including normalized mobility, on/off ratio, and hysteresis in $V_g$ are shown in Figure 5c, d, and e, respectively. Low-field mobility was impacted by less than 5% on average until ~1.5% strain. At about 2% strain, the average normalized mobility reduced by ~18% indicating a more pronounced performance degradation (Figure 5c). Similar trends were observed for the on/off ratio and voltage hysteresis. Although the average on/off ratio remained relatively stable under bending strain as is shown in Figure 5d, the standard deviation increased noticeably at the maximum applied strain of 2%. For hysteresis in $V_g$ (Figure 5e), the average value increased from ~0.3 V to ~0.4 V at strains up to 1.5% and to ~0.7 V at 2% strain. We attribute the observed degradation of BP device robustness at ~2% strain to the 25 nm $Al_2O_3$ dielectrics (bottom gate dielectric and top-side encapsulation), which is known to suffer from film degradation at tensile strains ~ ≥ 2%.[7] Moreover, 2% applied tensile strain is above the elastic-plastic transition point (i.e., yield strain) of the PI substrate; hence, the substrate cannot fully recover after release of the strain.[64] Residual strain in the PI substrate can result in increased interface trap charge in the gate dielectric, consequently leading to reduced mobility, on current, drain current modulation, and increased hysteresis.[65−67] We note that the mechanical robustness of BP devices can be further improved by utilizing flexible insulators such as two-dimensional h-BN and organic insulators,[4,5,8,68] as dielectric and passivation layers.

For practical flexible and bendable electronics, another important criteria is the device endurance under repeated



DOI: 10.1021/nl5047329
Nano Lett. 2015, 15, 1883−1890

bending. In this work, an RSA-G2 Dynamic Mechanical Analyzer (DMA) was used for multicycle three-point bending measurements. The DMA system setup is shown in the Supporting Information Figure S7 and the working scene can be seen in Supporting Information Video 2. A tensile strain of 1.5% was applied to the BP transistors. Then, 500 and 5000 cycles with bending frequency of 1 Hz were applied and no mechanical failure was observed. As is shown in Figure 5f, the transfer characteristics of the flexible BP transistors demonstrated strong stability even after 5000 cycles of bending. To further verify the robustness of flexible BP electronics, we remeasured the demodulator after 500 cycles of bending, showing that in addition to the current−voltage characteristics, the demodulation functionality was also preserved with similarly high demodulation efficiency. Electrical comparison of demodulator transistor performance including device transfer and output characteristics can be found in the Supporting Information Figure S8.

In summary, we have investigated semiconducting BP devices on flexible substrates for the first time and achieved high mobilities, inverting and noninverting amplifiers, and frequency doubler. The experimental BP transistors showed robust performance under mechanical bending up to ∼2% tensile strain and 5000 bending cycles. Larger mechanical strains can be accommodated by replacing commonly used high-k dielectric with flexible organic or polymeric gate dielectric. Furthermore, we demonstrated a flexible AM demodulator, enabled by a single BP ambipolar transistor. Our device results on polyimide represent the state-of-the-art in electronic performance among layered semiconductor flexible transistors.

## ■ ASSOCIATED CONTENT

### Supporting Information

Analysis details of black phosphorus crystal structure, anisotropic Raman spectra, long-term stability of flexible BP devices, statistics of mobility and drain current modulation of unstrained BP devices, inverter functionality, inverter gain, intrinsic gain of BP FET, flexible BP AM demodulator system setup, DMA auto bending system setup, and multicycle bending robustness of flexible BP AM demodulator are discussed in detail. Supporting videos that record music signal demodulation by flexible BP AM demodulator before and after multicycle bending test and DMA bending measurement are also provided. These materials are available free of charge via the Internet at http://pubs.acs.org.

## ■ AUTHOR INFORMATION

### Corresponding Author

*E-mail: deji@ece.utexas.edu.

### Author Contributions

The manuscript was written through contributions of all authors. All authors have given approval to the final version of the manuscript.

### Notes

The authors declare no competing financial interest.

## ■ ACKNOWLEDGMENTS

This work is supported in part by the Office of Naval Research (ONR) under contract N00014-1110190, and the NSF-NASCENT Engineering Research Center under Cooperative Agreement No. EEC-1160494.

## ■ REFERENCES

(1) Akinwande, D.; Petrone, N.; Hone, J. *Nat. Commun.* **2014**, 5678.
(2) Wang, Q. H.; Kalantar-Zadeh, K.; Kis, A.; Coleman, J. N.; Strano, M. S. *Nat. Nanotechnol.* **2012**, *7* (11), 699−712.
(3) Schwierz, F. *Proc. IEEE* **2013**, *101* (7), 1567−1584.
(4) Lee, J.; Ha, T. J.; Li, H.; Parrish, K. N.; Holt, M.; Dodabalapur, A.; Ruoff, R. S.; Akinwande, D. *ACS Nano* **2013**, *7* (9), 7744−50.
(5) Lee, J.; Ha, T. J.; Parrish, K. N.; Chowdhury, S. F.; Tao, L.; Dodabalapur, A.; Akinwande, D. *IEEE Electron Device Lett.* **2013**, *34* (2), 172−174.
(6) Petrone, N.; Meric, I.; Hone, J.; Shepard, K. L. *Nano Lett.* **2012**, *13*, 121−125.
(7) Chang, H. Y.; Yang, S.; Lee, J.; Tao, L.; Hwang, W. S.; Jena, D.; Lu, N.; Akinwande, D. *ACS Nano* **2013**, *7* (6), 5446−52.
(8) Lee, G. H.; Yu, Y. J.; Cui, X.; Petrone, N.; Lee, C. H.; Choi, M. S.; Lee, D. Y.; Lee, C.; Yoo, W. J.; Watanabe, K.; Taniguchi, T.; Nuckolls, C.; Kim, P.; Hone, J. *ACS Nano* **2013**, *7* (9), 7931−6.
(9) Li, L.; Yu, Y.; Ye, G. J.; Ge, Q.; Ou, X.; Wu, H.; Feng, D.; Chen, X. H.; Zhang, Y. *Nat. Nanotechnol.* **2014**, *9* (5), 372−7.
(10) Liu, H.; Neal, A. T.; Zhu, Z.; Luo, Z.; Xu, X.; Tomanek, D.; Ye, P. D. *ACS Nano* **2014**, *8* (4), 4033−41.
(11) Kobayashi, T.; Bando, M.; Kimura, N.; Shimizu, K.; Kadono, K.; Umezu, N.; Miyahara, K.; Hayazaki, S.; Nagai, S.; Mizuguchi, Y.; Murakami, Y.; Hobara, D. *Appl. Phys. Lett.* **2013**, *102* (2), 023112−4.
(12) Rahimi, S.; Tao, L.; Chowdhury, S. F.; Park, S.; Jouvray, A.; Buttress, S.; Rupesinghe, N.; Teo, K.; Akinwande, D. *ACS Nano* **2014**, *8* (10), 10471−9.
(13) Bae, S.; Kim, H.; Lee, Y.; Xu, X.; Park, J. S.; Zheng, Y.; Balakrishnan, J.; Lei, T.; Kim, H. R.; Song, Y. I.; Kim, Y. J.; Kim, K. S.; Ozyilmaz, B.; Ahn, J. H.; Hong, B. H.; Iijima, S. *Nat. Nanotechnol.* **2010**, *5* (8), 574−8.
(14) Kim, S.; Konar, A.; Hwang, W. S.; Lee, J. H.; Lee, J.; Yang, J.; Jung, C.; Kim, H.; Yoo, J. B.; Choi, J. Y.; Jin, Y. W.; Lee, S. Y.; Jena, D.; Choi, W.; Kim, K. *Nat. Commun.* **2012**, *3*, 1011.
(15) Cheng, R.; Jiang, S.; Chen, Y.; Liu, Y.; Weiss, N.; Cheng, H. C.; Wu, H.; Huang, Y.; Duan, X. *Nat. Commun.* **2014**, *5*, 5143.
(16) Ma, N.; Jena, D. *Phys. Rev. X* **2014**, *4* (1), 011043.
(17) Jin, Z. H.; Li, X. D.; Mullen, J. T.; Kim, K. W. *Phys. Rev. B* **2014**, *90* (4), 045422.
(18) Das, S.; Gulotty, R.; Sumant, A. V.; Roelofs, A. *Nano Lett.* **2014**, *14* (5), 2861−6.
(19) Mitzi, D. B.; Kosbar, L. L.; Murray, C. E.; Copel, M.; Afzali, A. *Nature* **2004**, *428* (6980), 299−303.
(20) Wei, C.-Y.; Shu-Hao, K.; Yu-Ming, H.; Wen-Chieh, H.; Adriyanto, F.; Yeong-Her, W. *IEEE Electron Device Lett.* **2011**, *32* (1), 90−92.
(21) Hsu, H. H.; Chang, C. Y.; Cheng, C. H. *IEEE Electron Device Letters* **2013**, *34* (6), 768−770.
(22) Nathan, A.; Ahnood, A.; Cole, M. T.; Lee, S.; Suzuki, Y.; Hiralal, P.; Bonaccorso, F.; Hasan, T.; Garcia-Gancedo, L.; Dyadyusha, A.; Haque, S.; Andrew, P.; Hofmann, S.; Moultrie, J.; Chu, D. P.; Flewitt, A. J.; Ferrari, A. C.; Kelly, M. J.; Robertson, J.; Amaratunga, G. A. J.; Milne, W. I. *Proc. IEEE* **2012**, *100* (Special Centennial Issue), 1486−1517.
(23) Hsu, H.-H.; Chang, C.-Y.; Cheng, C.-H. *IEEE Electron Device Letters* **2013**, *34* (6), 768−770.
(24) Li, Y. V.; Ramirez, J. I.; Sun, K. G.; Jackson, T. N. *IEEE Electron Device Letters* **2013**, *34* (7), 891−893.
(25) Morita, A. *Appl. Phys. A: Mater. Sci. Process.* **1986**, *39* (4), 227−242.
(26) Castellanos-Gomez, A.; Vicarelli, L.; Prada, E.; Island, J. O.; Narasimha-Acharya, K. L.; Blanter, S. I.; Groenendijk, D. J.; Buscema, M.; Steele, G. A.; Alvarez, J. V.; Zandbergen, H. W.; Palacios, J. J.; Van der Zant, H. S. J. *2D Materials* **2014**, *1* (2), 025001.
(27) Buscema, M.; Groenendijk, D. J.; Blanter, S. I.; Steele, G. A.; van der Zant, H. S. J.; Castellanos-Gomez, A. *Nano Lett.* **2014**, *14* (6), 3347−3352.
(28) Buscema, M.; Groenendijk, D. J.; Steele, G. A.; van der Zant, H. S. J.; Castellanos-Gomez, A. *Nat. Commun.* **2014**, *5*, 4651.



DOI: 10.1021/nl5047329
*Nano Lett.* 2015, 15, 1883−1890

(29) Deng, Y.; Luo, Z.; Conrad, N. J.; Liu, H.; Gong, Y.; Najmaei, S.; Ajayan, P. M.; Lou, J.; Xu, X.; Ye, P. D. *ACS Nano* **2014**, *8* (8), 8292−8299.
(30) Engel, M.; Steiner, M.; Avouris, P. *Nano Lett.* **2014**, *14* (11), 6414−6417.
(31) Hong, T.; Chamlagain, B.; Lin, W.; Chuang, H.-J.; Pan, M.; Zhou, Z.; Xu, Y.-Q. *Nanoscale* **2014**, *6* (15), 8978−8983.
(32) Tran, V.; Soklaski, R.; Liang, Y. F.; Yang, L. *Phys. Rev. B* **2014**, *89* (23), 235319.
(33) Nayfeh, O. M. *IEEE Electron Device Letters* **2011**, *32* (10), 1349−1351.
(34) Yeh, C. H.; Lain, Y. W.; Chiu, Y. C.; Liao, C. H.; Moyano, D. R.; Hsu, S. S.; Chiu, P. W. *ACS Nano* **2014**, *8* (8), 7663−70.
(35) Xia, F.; Wang, H.; Jia, Y. *Nat. Commun.* **2014**, *5*, 4458.
(36) Zhang, S.; Yang, J.; Xu, R.; Wang, F.; Li, W.; Ghufran, M.; Zhang, Y. W.; Yu, Z.; Zhang, G.; Qin, Q.; Lu, Y. *ACS Nano* **2014**, *8* (9), 9590−6.
(37) Qiao, J.; Kong, X.; Hu, Z. X.; Yang, F.; Ji, W. *Nat. Commun.* **2014**, *5*, 4475.
(38) Wood, J. D.; Wells, S. A.; Jariwala, D.; Chen, K. S.; Cho, E.; Sangwan, V. K.; Liu, X.; Lauhon, L. J.; Marks, T. J.; Hersam, M. C. *Nano Lett.* **2014**, 6964−6970.
(39) Kim, J.-S.; Liu, Y.; Zhu, W.; Kim, S.; Wu, D.; Tao, L.; Dodabalapur, A.; Lai, K.; Akinwande, D. Toward Air-Stable Multilayer Phosphorene Thin-Films and Transistors. 2014, *arXiv:1412.0355*. arXiv.org e-Print archive. http://arxiv.org/abs/1412.0355 (accessed Jan 2015).
(40) Tao, L.; Lee, J.; Akinwande, D. *J. Vac. Sci. Technol., B: Nanotechnol. Microelectron.: Mater., Process., Meas., Phenom.* **2011**, *29* (6), -.
(41) Popov, I.; Seifert, G.; Tománek, D. *Phys. Rev. Lett.* **2012**, *108* (15), 156802.
(42) Das, S.; Demarteau, M.; Roelofs, A. *ACS Nano* **2014**, *8* (11), 11730−8.
(43) Cai, Y.; Zhang, G.; Zhang, Y. W. *Sci. Rep.* **2014**, *4*, 6677.
(44) Chang, H. Y.; Zhu, W.; Akinwande, D. *Appl. Phys. Lett.* **2014**, *104* (11), -.
(45) Du, Y.; Liu, H.; Deng, Y.; Ye, P. D. *ACS Nano* **2014**, *8* (10), 10035−42.
(46) Li, S. L.; Miyazaki, H.; Kumatani, A.; Kanda, A.; Tsukagoshi, K. *Nano Lett.* **2010**, *10* (7), 2357−62.
(47) Guerriero, E.; Polloni, L.; Rizzi, L. G.; Bianchi, M.; Mondello, G.; Sordan, R. *Small* **2012**, *8* (3), 356−61.
(48) Wang, H.; Wang, X.; Xia, F.; Wang, L.; Jiang, H.; Xia, Q.; Chin, M. L.; Dubey, M.; Han, S. J. *Nano Lett.* **2014**, *14* (11), 6424−9.
(49) Ramón, M. E.; Parrish, K. N.; Chowdhury, S. F.; Magnuson, C. W.; Movva, H. C. P.; Ruoff, R. S.; Banerjee, S. K.; Akinwande, D. *IEEE Trans. Nanotechnol.* **2012**, *11* (5), 877−883.
(50) Han, S. J.; Jenkins, K. A.; Valdes Garcia, A.; Franklin, A. D.; Bol, A. A.; Haensch, W. *Nano Lett.* **2011**, *11* (9), 3690−3.
(51) Gray, P. R.; Hurst, P. J.; Meyer, R. G.; Lewis, S. H. *Analysis and design of analog integrated circuits*; John Wiley & Sons: Hoboken, NJ, 2008.
(52) Razavi, B. *Solid-State Circuits, IEEE Journal of* **1999**, *34* (3), 268−276.
(53) Parrish, K. N.; Akinwande, D. *Appl. Phys. Lett.* **2011**, *99* (22), -.
(54) Wang, H.; Nezich, D.; Kong, J.; Palacios, T. *IEEE J. Solid-State Circuits* **2009**, *30* (5), 547−549.
(55) Fan, J.; Yuen, J. D.; Wang, M.; Seifter, J.; Seo, J. H.; Mohebbi, A. R.; Zakhidov, D.; Heeger, A.; Wudl, F. *Adv. Mater.* **2012**, *24* (16), 2186−90.
(56) Wang, H.; Hsu, A.; Ki Kang, K.; Kong, J.; Palacios, T. Gigahertz ambipolar frequency multiplier based on CVD graphene. *Proc. IEEE Electron Devices Meet.* **2010**, 23.6.1−23.6.4.
(57) Rutherglen, C.; Burke, P. *Nano Lett.* **2007**, *7* (11), 3296−3299.
(58) Zhu, W. J.; Farmer, D. B.; Jenkins, K. A.; Ek, B.; Oida, S.; Li, X. S.; Bucchignano, J.; Dawes, S.; Duch, E. A.; Avouris, P. *Appl. Phys. Lett.* **2013**, *102* (23), 233102.
(59) Fei, R.; Yang, L. *Nano Lett.* **2014**, *14* (5), 2884−9.
(60) Elahi, M.; Khaliji, K.; Tabatabaei, S. M.; Pourfath, M.; Asgari, R. Modulation of electronic and mechanical properties of phosphorene through strain. 2014, *arXiv:1407.7706*. arXiv.org e-Print archive. http://arxiv.org/abs/1407.7706 (accessed Jan 2015).
(61) Wei, Q.; Peng, X. H. *Appl. Phys. Lett.* **2014**, *104* (25), 251914.
(62) Kim, K. S.; Zhao, Y.; Jang, H.; Lee, S. Y.; Kim, J. M.; Kim, K. S.; Ahn, J. H.; Kim, P.; Choi, J. Y.; Hong, B. H. *Nature* **2009**, *457* (7230), 706−10.
(63) Argon, A. S.; Bessonov, M. *Philos. Mag.* **1977**, *35* (4), 917−933.
(64) Lee, E. H. *J. Appl. Mech.* **1969**, *36* (1), 1−6.
(65) Hook, T. B.; Ma, T. *Appl. Phys. Lett.* **1986**, *48* (18), 1208−1210.
(66) Zhu, W. J.; Ma, T. P.; Zafar, S.; Tamagawa, T. *IEEE Electron Device Lett.* **2002**, *23* (10), 597−599.
(67) Yeh, W. K.; Wang, C. C.; Hsu, C. W.; Fang, Y. K.; Wu, S. M.; Ou, C. C.; Lin, C. L.; Gan, K. J.; Weng, C. J.; Chen, P. Y.; Jiann-Shiun, Y.; Liou, J. J. Impact of oxide trap charge on performance of strained fully depleted SOI metal-gate MOSFET. *IEEE Int. Conf. Electron Devices Solid-State Circuits* **2009**, 197−200.
(68) Klauk, H.; Halik, M.; Zschieschang, U.; Eder, F.; Rohde, D.; Schmid, G.; Dehm, C. *IEEE Trans. Electron Devices* **2005**, *52* (4), 618−622.


DOI: 10.1021/nl5047329
*Nano Lett.* 2015, 15, 1883−1890